Visible Light Photoinitiation of Cell Adhesive Gelatin Methacryloyl Hydrogels for Stereolithography 3D Bioprinting

Zongjie Wang[1, #], Zhenlin Tian[2], Xian Jin[1], Jonathan F. Holzman[1], Frederic Menard[2], and Keekyoung Kim[1, 3, *]

[1]School of Engineering, University of British Columbia, Kelowna, BC, V1V 1V7, Canada

[2]Irving K. Barber School of Arts and Sciences, University of British Columbia, Kelowna, BC, V1V 1V7, Canada

[3]Biomedical Engineering Program, University of British Columbia, Vancouver, BC, V6T 1Z4, Canada

[#]Current address: The Edward S. Rogers Sr. Department of Electrical and Computer Engineering and Leslie Dan Faculty of Pharmacy, University of Toronto, Toronto, ON, M5S 3M2, Canada

*Corresponding author: Dr. Keekyoung Kim, email: keekyoung.kim@ubc.ca

Abstract

We present the first cell attachable and visible light crosslinkable hydrogels based on gelatin methacryloyl (GelMA) with eosin Y (EY) photoinitiation for stereolithography 3D bioprinting. In order to develop visible a light crosslinkable hydrogel, we systematically studied five combinations of the GelMA and EY photoinitiator with various concentrations. Their mechanical properties, microstructures, and cell viability and confluency after encapsulation were investigated rigorously to elucidate the effects of the EY and GelMA macromer concentration on the characteristics of the hydrogel. Experimental results show that the compressive Young's Modulus and pore size are positively affected by the concentration of EY, while the mass swelling ratio and cell viability are negatively affected. Increasing the concentration of GelMA helps to improve the compressive Young's Modulus and cell attachment. We further employed the developed visible light-based stereolithography bioprinting system to print the patterned cell-laden hydrogels to demonstrate the bioprinting applications of the developed hydrogel. We observed good cell proliferation and the formation of a 3D cellular network inside the printed pattern at day 5, which proves the great feasibility of using EY-GelMA as the bioinks for biofabrication and tissue engineering.

Key words: Visible light crosslinking, Gelatin methacryloyl hydrogel, Eosin Y, Stereolithography, 3D Bioprinting

1. Introduction

Hydrogels are important biomaterials in biotechnology and bioengineering because of their excellent biocompatibility, high swelling ratio, and good permeability for water-soluble metabolites [1]. Hydrogels have been extensively used in tissue engineering and regenerative medicine, including biomarker detection [2], stem cell study [3], and organ-on-a-chip applications [4]. Among all hydrogels, photopolymerizable hydrogels have received substantial attention due to the high controllability during polymerization, fast curing rates at physiological temperatures, minimal heat production, and minimal invasiveness to *in situ* hydrogel structures [1].

Photopolymerization generally utilizes photoinitiators which have an absorption peak at a specific wavelength to start radical initiating species [1]. For biomedical applications, the photoinitiators need to be biocompatible, water-soluble and low in cytotoxicity. In Table 1, we list the most widely used photoinitiators in tissue engineering. The majority of photoinitiators works within the ultra-violet (UV) wavelength band (between 250 nm and 400 nm). However, it has been reported extensively that the UV irradiation can induce damage to the cells' DNA [5,6], and cancerization of the skin [5,7]. Thus, it is safer to use visible light sensitive photoinitiators for polymerization. Recently, several groups have reported that LAP (lithium phenyl-2,4,6-trimethylbenzoylphosphinate) and VA-086 (2,2'-azobis[2-methyl-n-(2-hydroxyethyl)propionamide]) initiator could also be initiated by

near-UV blue light (~ 405 nm) [8,9], but it was shown that strong 405 nm blue light was also toxic to mammal cells and disruptive to cellular processes [10]. Therefore, photoinitiators with the absorbing peak higher than the blue light wavelength (higher than 405 nm) are preferred. With this in mind, eosin Y (EY)-based photoinitiation has been reported to be a green light sensitive (wavelength between 500 nm to 600 nm) and highly biocompatible crosslinking solution for tissue engineering [11]. EY-based photoinitiation has also been used with polyethylene glycol diacrylate (PEGDA) [11] and PEGDA-GelMA hybrid hydrogels [12], which are non-adhesive to cells. The attachment of cells to their surrounding microenvironments is essential for them to maintain their function and integrity [13–15]. Thus, the visible light-based photoinitiation of cell-adhesive hydrogels is desired for tissue and organ regeneration.

In recent years, bioprinting has become a promising technique to generate 3D tissue-like structures for tissue regeneration and disease study [16,17]. Bioprinting has successfully generated many artificial tissues, including cartilage [18], vessel [19], bone [20] and even complex heterogeneous tissues containing different cell types and extra-cellular matrices [21,22]. Among all bioprinting techniques, stereolithography (SLA) 3D bioprinting has many advantages over traditional extrusion or inkjet-based bioprinting [17]. In SLA 3D bioprinting systems, photocrosslinkable hydrogels are selectively solidified in a layer-by-layer manner that additively builds up 3D structures. This technique uses a digital mirror

array to control the light pattern in the field of projection for selectively crosslinking each layer of the hydrogel prepolymer solution at a time. Such SLA bioprinting is reproducible and fast. Also, the resolution of the printed pattern depends on the size of each micromirror (usually around 25 – 100 μm), which is typically better than those of extrusion-based 3D bioprinting systems. In addition, because there is no external force applied to the cells during printing, the SLA 3D bioprinting ensures high cell viability. Taking the advantages of high speed, high cell viability, and high resolution, the SLA 3D bioprinting has been utilized to fabricate heterogeneous tissues for engineering cell-cell interaction [23], porous 3D tissue scaffolds [24], microscale cancer tissues for cancer cell migration study [25] and *in vitro* hepatic models for drug discovery and disease study [26]. However, most of the SLA 3D bioprinting systems rely on UV light [24–26] or near-UV blue light (405 nm) [27]. Replacing the light source with visible light may reduce the potential risk of carcinogenesis, due to the long UV exposure time during printing, which allows tissue scaffolds to be fabricated in a safe manner.

In this paper, we present results on visible light crosslinkable and cell-adhesive gelatin methacryloyl (GelMA) bioinks using EY photoinitiation for a visible light-based SLA 3D bioprinting system. We systematically study the system to determine the critical concentration of EY for crosslinking of 10%, 15%, and 20% w/v GelMA hydrogels, as well as study the effect of EY concentration on the mechanical properties, microstructure, cell

viability, and cell adhesion of the GelMA hydrogels. We employ the visible light-based SLA 3D bioprinting system to print a cell-laden mesh pattern, demonstrating that EY-GelMA hydrogels have great potential as a bioink for future 3D bioprinting and tissue regeneration applications.

2. Materials and methods

2.1 Bioprinting system design and working principle

The proposed bioprinting system is a modified version of our previously reported system [12]. As shown in Figure 1A, the system consists of three main components: a beam projector, a filter system, and a syringe pump. The beam projector (HD6510BD, Acer, Taipei, Taiwan), which is located 4 cm away from a reflection mirror, provided the patterned illumination for the SLA 3D bioprinting. The distance between the mirror and printing plane was approximately 6 cm. A 4 cm thick water filter was located between the mirror and the printed sample to filter the harmful infrared radiation and heat generated by the lamp of the projector. A syringe pump (Genie Touch, Kent Scientific, Torrington, CT, USA) was utilized to automatically add the bioinks before the printing of each layer. The light spectrum of the lamp was characterized using a compact spectrometer (CCS200, Thorlabs, Newton, NJ, USA) within the printing plane.

Based on the input from a computer, the beam projector controls the brightness of each

projected pixel and generates an array of white and black points. This array of light is reflected and focused by a lens system and passes through the water filter [12]. The filtered lights are directly projected onto a photocrosslinkable hydrogel prepolymer solution. Depending on the brightness of the light, specific areas of the hydrogel forms 3D printed patterns. This SLA-based bioprinting is a layer-by-layer fabrication method. Thus, to fabricate a complex structure in the vertical direction, another layer of hydrogel prepolymer solution is added through a syringe pump.

The selective crosslinking mechanism of one layer is illustrated in Figure 1B. Inside the beam projector, there is a microfabricated micromirror array that is referred to a digital micromirror device (DMD). One micromirror of the DMD represents a pixel of the computer screen. The DMD can control the angle of the mirror, which determines the brightness of the light reflecting from the mirror. Therefore, DMD array is able to control the light intensity of each pixel. In the DMD array, the green color means that the pixels are white in color (being a high intensity) while the black means that the pixels are black in color (being a low intensity). The light beams generated by the DMD array are passed through the lens system to focus the light beam onto the printing area. With such a lens system, the beam projector can clearly focus objectives on the printing plane. In the area exposed by the white light, the visible light sensitive photoinitiator is triggered to start free radical-based polymerization while the area exposed by the black light cannot undergo

such a process. As a result, the system is able to selectively crosslink patterns in each layer. In this study, the field of view at the printing plane is approximately 9.6 × 5.4 cm and the minimum feature size is roughly 50 μm, as we previously reported [12].

2.2 Hydrogel preparation and characterization

GelMA hydrogel was synthesized by the process described in [28]. Briefly, 5 g of gelatin was dissolved in 50 mL of dimethyl sulfoxide (BDH Chemicals, Radnor, PA, USA) at 50ºC. Then, 0.3 g of 4-dimethylaminopyridine (Sigma-Aldrich, St. Louis, MO, USA) and 2 mL of glycidyl methacrylate (Sigma-Aldrich, St. Louis, MO, USA) were sequentially added to the mixture. The mixture was allowed to react by stirring for two days at 50ºC. After the synthesis steps, the mixture was dialyzed with reverse osmosis (RO) water at room temperature for 7 days by changing the water twice a day. After dialysis, the dried sample was formed via lyophilization.

The preparation process of the EY based photoinitiator was adapted from Bahney *et al.* [11]. The base concentration of the reagents was 0.01 mM eosin Y disodium salt, 0.1% w/v triethanolamine (TEA), and 37 nM 1-vinyl-2 pyrrolidinone (NVP). All materials were purchased from Sigma-Aldrich, St. Louis, MO, USA. First, we prepared the mixture of 0.1 mM EY, 1% w/v TEA, and 370 nM NVP with phosphate buffered saline (PBS), which is a 10 times (10X) concentrated stock solution. Amounts of freeze-dried GelMA were

dissolved in different volumes of 10X EY photoinitiator solution and PBS to achieve five combinations of hydrogel pre-polymer solutions (i.e., 4X EY 10% GelMA, 2X EY 15% GelMA, 3X EY 15% GelMA, 4X EY 15% GelMA, and 1X EY 20% GelMA, as shown in Table 2). More combinations of GelMA and EY mixtures were also tested to determine the crosslinkability of the hydrogels.

Absorption spectra of the EY based photoinitiator were measured by a UV-Vis spectrophotometer (UV-2550, Shimadzu, Kyoto, Japan). The results are shown as a function of wavelengths ranging from 300 nm to 800 nm in Figure 2. A 2X EY 15% GelMA prepolymer solution sample was prepared as described in section 2.2. A blank PBS solution sample, only containing 15% w/v GelMA solution, was also prepared as a spectra reference.

To test mechanical properties, 5 mL of each type of EY GelMA prepolymer solution was pipetted into a petri dish at 6 cm in diameter and exposed to the light generated by the SLA 3D bioprinting system for 10 minutes to allow the full crosslinking of the hydrogel. The petri dish was placed 6 cm away from the light bulb. Five cylindrical specimens (12.7 mm in diameter) from each type of EY-GelMA hydrogels were punched from the petri dish. The compressive Young's modulus of each sample was tested by a dynamic mechanical analysis (DMA) instrument (Q800, TA Instruments, New Castle, DE, USA). The compressive modulus was determined as the slope of the linear region between strains from

5% to 20%.

For the measurement of mass swelling ratios, five cylindrical specimens were prepared using the method described above and the samples' residual liquid was removed by a paper tissue. Then, the swollen weight of the sample was measured using an analytical precision balance (Sartorius, Mississauga, ON, Canada). Subsequently, those samples were lyophilized under -45ºC for five days to determine the dry weight of the samples. The mass swelling ratio was calculated by the following formula:

$$\text{Mass swelling ratio} = \frac{\text{Swollen weight of the sample}}{\text{Dry weight of the sample}}$$

We examined the microstructure of the samples coated with 10 nm of gold/palladium (Au/Pd) alloy by sputtering. Microstructural images of each sample were taken by a scanning electron microscope (Mira3 XMU, TESCAN, Brno, Czech Republic).

2.3 Cell culturing and encapsulation

NIH 3T3 fibroblasts cells were cultured at 37ºC under a 5% CO_2 atmosphere**.** The cell media consists of Dulbecco's Modified Eagle Medium (Lonza, Basel, Switzerland) supplemented with 10% v/v heat-inactivated fetal bovine serum (Thermo Fisher Scientific, Waltham, MA, USA), and 1% v/v penicillin-streptomycin (Sigma-Aldrich, St. Louis, MO,

USA).

Each type of EY GelMA prepolymers was mixed with NIH 3T3 fibroblasts ($3x10^6$ cells/mL) before the crosslinking process. Then, 100 μL of each type of EY GelMA prepolymer with cells was evenly pipetted to a petri dish (3.5 cm in diameter) to form a hemispherical droplet. The droplet was then exposed to green light generated by the SLA 3D bioprinting system for 20 minutes. We set the distance between the petri dish and the bulb at 6 cm. Immediately after printing, the sample was washed with PBS twice. Subsequently, we added 3 mL of fresh media to the petri dish and placed it into the incubator for further culturing.

We examined the cell proliferation and morphology at day 1, day 4, and day 6. Crosslinked hemispherical droplet samples were washed two times with PBS and treated with a live/dead assay (Biotium, Hayward, CA, USA) for 30 minutes. Subsequently, we observed the assayed samples under a confocal fluorescence microscope (FV1000, Olympus, Tokyo, Japan). We used a 10X objective and two fluorescent channels (FITC and Texas Red) to capture the microscope image. Z-stacked cross-sections image images were acquired with 20 μm between each step. Fluoview software (version 3.1a, Olympus, Tokyo, Japan) was used to stack the images.

To analyze the cell viability, the fluorescent images taken by the microscope at day 1 were converted to a 16-bit gray value format, and the number of live cells was counted manually to calculate the cell viability. We also compared the cell coverage between day 1 and day 6 to evaluate the confluency of cells. The green channel of the fluorescent images taken by the microscope at day 1 and day 6 was converted to a 16-bit gray value format and normalized through a histogram equalization function (histeq) in the image processing toolkit provided by MATLAB 2014b (Mathworks, Natick, MA, USA). Then, a threshold gray value was set to filter at pixels with brightness lower than the threshold. Through this threshold filtering, only the pixels with high brightness for the green fluorescent signal, or equivalently, the pixels stained by Calcein AM, remained. Then the cell coverage was calculated by the following expression:

$$\text{Cell coverage} = \frac{\text{Area size of bright pixels}}{\text{Area size of the entire field of view}}$$

2.5 Bioprinting experiments

Figure 1C presents the process of 3D SLA bioprinting which is based on single layer patterning. Briefly, after patterning of the first layer, another layer of prepolymer solution was added onto the first layer in the petri dish by a syringe pump. Then, the patterning of the second layer was started. Such adding and patterning in a layer-by-layer process was repeated until an entire 3D structure was built. The crosslinking time was controlled

precisely to ensure that only the newly-added layer was crosslinked while the uncrosslinked area in the previous layer was not significantly affected by a consecutive printing process. In the end, the uncrosslinked prepolymer solution was removed and only the bioprinted structure remained in the petri dish. In this paper, 2X EY 15% GelMA hydrogel was employed to print the patterned shapes for the demonstration of 3D bioprinting.

For printing cell-laden 3D structures, the 2X EY 15% GelMA prepolymer was mixed with NIH 3T3 fibroblasts ($8x10^6$ cells/mL) to prepare a bioink before the bioprinting process. Subsequently, 1 mL of the bioink was evenly added to a petri dish (3.5 cm in diameter) to form a uniform and thin layer of the bioink. The petri dish was then exposed to the patterned light coming out of the beam projector for 4 minutes to print a bottom layer of the pattern. Then, 200 μL of the bioink was added into the petri dish and exposed to the light for 2 minutes. This process was repeated until the desired 3D structure was completed. Immediately after printing, the sample was washed with PBS twice and 3 mL of fresh media was added to the petri dish for culturing the 3D printed sample in the incubator.

The cell distribution and morphology of the bioprinted sample were examined at day 5 via DAPI/Phalloidin staining. The detailed protocol is as follows. The cultured samples were washed with PBS three times to remove the media. Then, 3.7% v/v paraformaldehyde

(Sigma-Aldrich, St. Louis, MO, USA) diluted in PBS was added to fix the samples for 15 minutes at room temperature and washed away with PBS. The samples were treated with 0.5% v/v Triton-X 100 diluted in PBS for 8 minutes and washed with PBS. Then, a 100 nM stock solution of Phalloidin 488 (Cytoskeleton, Denver, CO, USA) was added to the samples for incubating at room temperature for 60 minutes to stain the F-actin of the cells. In the end, the samples were washed with PBS three times and mounted by mounting media with DAPI (Sigma-Aldrich, St. Louis, MO, USA). The fluorescently labeled samples were then examined under a fluorescence microscope (DMi8, Leica, Wetzlar, Germany). We used a 5X objective with two fluorescent channels (DAPI and GFP) to visualize the printed mesh pattern. Also, a confocal fluorescence microscope (FV1000, Olympus) with 10X and 40X objective was used to obtain 3D cellular network images inside the printed samples.

2.6 Statistical analysis

A one-way analysis of variance (ANOVA analysis) function in MATLAB was used to statistically analyze the data pertaining to mechanical properties, swelling ratio, cell viability and coverage. Results are shown as an average ± standard deviation.

3. Results and discussion

3.1 Crosslinkability of GelMA with EY photoinitiator

To crosslink the hydrogel, a photocrosslinking system needs to have a water-soluble

photoinitiator to initiate polymerization. Such widely used photoinitiators include Irgacure 2959, LAP, VA-086 and EY [29] (Table 1). These initiators can be further divided into two categories according to the free radical generation mechanisms. On the one hand, cleavable photoinitiators (type-I) undergo cleavage from the excited triplet state and then release two free radicals. The type-I photoinitiators do not require any supplementary compound and have high initiation efficiency (e.g. Irgacure 2959, LAP, and VA-086). On the other hand, a bimolecular photoinitiating mechanism (type-II) is much more complex. It includes at least two components for a multi-step photoinitiation: a photosensitizer (i.e., EY) and an initiator (i.e., TEA). After illumination, the photosensitizer undergoes a fast electron transfer and a slow proton transfer process, providing the H-donor radical for polymerization [29]. Type-II photoinitiators (or photoinitiation systems) are much less efficient due to background electron transfers and solvent cage effect in aqueous solutions [30]. However, to our knowledge, there is currently no type-I photoinitiator that is compatible with visible lights, except near-UV blue light with the wavelength of 405 nm. In fact, using such blue light for the visible light-based SLA bioprinting is expensive and does not have a significant advantage over the current UV system. This is because of the following two reasons. First, the lamp in the commercial visible light beam projector cannot generate sufficiently strong blue light for illumination, as determined by the spectrum measurement result given in Figure 2A. Thus, producing strong blue light requires a specially-designed and expensive lamp. Second, strong blue light has been

reported to be harmful to mammal cells and disruptive to cellular processes [10]. Therefore, to build a visible light photoinitiation with better biocompatibility and without harmful effects, type-II photoinitiators are a more practical choice.

EY is a type-II photoinitiator system with the strongest absorption peak in the green light range. When we measured the absorption spectra of EY in GelMA hydrogel, we found that its absorption peak is located between 520 and 525 nm while most of the absorption occurs in the range of wavelengths from 500 to 550 nm (Figure 2B). As characterized before, the bioprinting system can generate a high intensity of light within the range of wavelengths from 500 to 550 nm (Figure 2A). Therefore, the EY photoinitiation can be effectively triggered by the visible light-based SLA bioprinting system.

Bahney *et al.* demonstrated that the optimum concentration of EY for good crosslinkability and cell viability of polyethylene (glycol) diacrylate (PEGDA) hydrogel was 0.01 mM EY, 0.1% w/v TEA and 37 nM NVP [11]. However, the PEGDA does not promote cell adhesion, which limits its application for tissue engineering. Thus, GelMA was mixed with PEG to improve the biocompatibility and cell adhesion property [31,32]. We found that GelMA mixed with PEGDA could be crosslinked with the optimum concentration of EY, although it takes a longer time to achieve a crosslinked hydrogel with higher concentrations of the GelMA [12]. Moreover, the pure GelMA prepolymer could not be properly crosslinked

with the optimum concentration of EY [12]. Considering the low efficiency of type-II photoinitiators, we hypothesized that a higher concentration of photoinitiator would be required to trigger photocrosslinking of the GelMA prepolymer. However, the higher concentration of EY and TEA negatively affected the cell viability [11]. Occhetta *et al.* also showed that simply increasing the concentration of GelMA macromer without changing the concentration of photoinitiator improved the crosslinkability of hydrogels [33]. Taken these claims into consideration, we added 1X, 2X and 4X concentrated EY photoinitiators to 10%, 15% and 20% w/v GelMA prepolymer solution to test their crosslinkability after 10 minutes' exposure to the visible light from the beam projector.

As can be seen in Table 3, 10% GelMA prepolymer solution required at least four times more EY for efficient crosslinking. The minimum ratios of EY required to crosslink 15% and 20% GelMA were 2X and 1X, respectively. With increasing GelMA concentration, less concentrated EY was required for crosslinking, as shown in Table 2. We next tested five different combinations of EY and GelMA (i.e., 1X EY 20% GelMA, 2X EY 15% GelMA, 4X EY 10% GelMA, 3X EY 15% GelMA, and 4X EY 15% GelMA) to study the effects of the GelMA macromer and EY concentrations on the physical and biological properties of GelMA hydrogels. The results are discussed below.

3.2 Physical properties of EY-GelMAs

Physical properties of hydrogels are key factors for cell proliferation and differentiation. It has been found that the shear modulus significantly affects the increment of chondrogenic differentiation [34]. The swelling ratio is also an essential parameter of hydrogels because it affects the cellular microenvironments, through properties such as surface mobility and solute diffusion [35]. In addition, the microstructure of hydrogels, especially the pore size, has been reported to be an important factor for cell attachment and growth [36]. Therefore, we systematically investigated the compressive Young's Modulus, mass swelling ratio, and microstructure of the EY GelMA hydrogels using the visible light-based SLA bioprinting system.

Figure 3 shows the various mechanical properties due to different macromer concentrations of the GelMA hydrogels crosslinked by the minimum concentrations of EY photoinitiator. The compressive Young's Modulus of 4X 10%, 2X 15% and 1X 20% GelMA was 4.40 kPa, 10.54 kPa and 14 kPa, respectively (Figure 3B). (Yue *et al.* stated that GelMA hydrogel was a relatively 'soft' hydrogel with Young's Modulus values less than 30 kPa without mixing other hydrogels [37].) Interestingly, the Young's Modulus of the GelMA crosslinked by the EY photoinitiator and visible light was slightly lower than those UV crosslinked by Irgacure 2959 [28] or VA-086 [38]. This observation may be explained by the low efficiency of the EY photoinitiator comparing to Irgacure 2959. As shown in Figure 3C, the mass swelling ratios of 4X 10%, 2X 15% and 1X 20% GelMAs were 7.45, 5.14

and 4.09, respectively. The mass swelling ratio of 4X 10% GelMA is similar to that of Irgacure 2959 crosslinked with 10% GelMA [28] and significantly greater than that of the EY crosslinked hybrid PEG-GelMA hydrogel [12]. Figures 3D – 3F present the scanning electron microscope (SEM) images of the microstructure of 4X 10%, 2X 15% and 1X 20% GelMA, respectively. The pore size of 2X 15% and 1X 20% GelMA (> 50 μm) were significantly greater than that of 4X 10% GelMA (< 50 μm), which may benefit the cell adhesion and proliferation, as reported by Murphy *et al.* [39].

We characterized the 15% GelMA hydrogels crosslinked with varying concentrations of EY photoinitiator to study its effect on the physical properties of GelMA hydrogels, as shown Figure 4. The compressive Young's Modulus of 2X 15%, 3X 15% and 4X 15% GelMA were 10.54 kPa, 11.98 kPa and 12.86 kPa, respectively (Figure 4B). The mass swelling ratios of 2X 15%, 3X 15% and 4X 15% GelMA resulted in 5.14, 5.12 and 4.92, respectively (Figure 4C). Thus, the results demonstrate that the concentration of EY positively affects the compressive Young's Modulus but negatively affects the mass swelling ratio of the GelMA hydrogels. In addition, Figures 4D – 4F show the SEM images of the microstructure of 2X 15%, 3X 15%, and 4X 15% GelMA hydrogels, respectively. It can be seen that higher concentrations of EY result in smaller pore sizes of the GelMA hydrogels. It can be concluded that EY GelMA hydrogels crosslinked by visible light are softer than the widely used Irgacure 2959/UV-based GelMA hydrogels, but these physical

properties can be tuned by changing the concentration of the GelMA macromer or EY photoinitiator.

3.3 Biocompatibility of EY-GelMAs

The mechanical properties of GelMA are not superior to those of other hydrogels, yet it remains still one of the most widely used hydrogels in tissue engineering because of its low cost and biocompatibility [37]. Cells attach and proliferate well in 2D and 3D GelMA hydrogel networks [28,38,40]. For these reasons, GelMA also has been widely applied to stem cell culturing and differentiation studies [41,42]. In tissue engineering, the capability of cell adhesion, proliferation, and migration in the 3D environment is critical for mimicking the *in vivo* tissue environment [43,44]. We encapsulated and cultured cells in the fine different combinations of GelMA and EY to test the effects of GelMA and EY concentration on the cell viability and adhesion at day 1, day 4 and day 6 for visible light-based 3D bioprinting applications.

Figure 5A shows representative images of live (Calcein AM: green) and dead (EthD-III: red) assay staining of cell-laden GelMA samples acquired with a confocal fluorescence microscope. At day 1, there were more dead cells (red dots) found in 4X 10% GelMA than the other two conditions. Some cells attached and elongated within the 1X 20% GelMA matrix, while none attached with 4X 10% GelMA. At day 4 and day 6, more cells were

found in 1X 20% GelMA than the other two conditions. This phenomenon indicates that the 1X 20% GelMA is the most biocompatible combination. Using image processing, we quantitatively analyzed cell viability at day 1 and cell confluency by quantifying the difference of cell coverage between day 1 and day 6. As shown in the Figure 5B, the cell viabilities of 1X 20%, 2X 15%, and 4X 10% GelMA were 91.5%, 85.9% and 75.6%, respectively. This result revealed that too much EY has a negative effect on cell viability after crosslinking, which correlates with a previous study [11]. At the same time, the difference in cell coverage at day 6 was significant among 1X 20%, 2X 15% and 4X 10% GelMA. The cells proliferated well and covered much larger area in 1X 20% GelMA as compared to the other two conditions. The superior cell coverage rate of 1X 20% GelMA can be explained by the following two reasons. First, the concentration of EY photoinitiator was shown to negatively affect the cell viability at day 1 and thus there were more live cells to proliferate with 1X 20% GelMA than with 2X 15% and 4X 10% GelMAs over several days' culture. Second, it has been widely reported that the cell proliferation is positively affected by the macromer concentration of GelMA [28,31,40].

Cell encapsulation and proliferation of 2X 15%, 3X 15% and 4X 15% GelMAs were also tested for 3D bioprinting applications as shown in Figure 6. Within this group, the GelMA macromer concentration was fixed to isolate the effect of EY concentration. Based on the fluorescent images and their quantitative analysis, 4X 15% GelMA showed significantly

lower cell viability at day 1 and lower cell proliferation at day 6 than the other two conditions (Figures 6A, 6B, and 6C). Therefore, adding more EY than the minimum concentration for triggering crosslinking with each macromer concentration of GelMAs can negatively affect the cell viability and proliferation after printing.

3.4 Bioprinting with EY-GelMA

The above characterization of physical properties and biocompatibility show that EY-GelMA can be properly crosslinked by visible light generated by a beam projector and that the cells can proliferate healthily inside the hydrogel. To demonstrate the 3D bioprinting application of EY-GelMA hydrogel, we utilized our visible light-based SLA 3D bioprinting system to print cell-laden EY-GelMA structures with a selection of patterns.

For these experiments, we applied the optimal combination of 2X 15% GelMA reagents. To demonstrate the capability of the visible light-based SLA bioprinting system to print various EY-GelMA patterns, a maple leaf and cone patterns of EY-GelMA hydrogel were printed (Figure 7). After the printing, the samples were colored by food dye to visualize the patterns. As can be seen in Figures 7A-D, the printed patterns were clear and had high structural integrity. As discussed in the previous sections, the lowest concentration of EY provided better cell viability after printing. Thus, 2X 15% GelMA was chosen rather than 3X or 4X 15% GelMAs. Also, 4X 10% GelMA showed relatively low cell viability, as compared to that of 2X 15% GelMA, while 1X 20% GelMA was too viscous and difficult

to handle. Ultimately, we chose to use 2X 15% GelMA, because it offers a good balance between cell viability, and proliferation, and the ease of handling during experiments.

A NIH-3T3 cell-laden 4x4-mesh pattern was also printed using the visible light-based SLA 3D bioprinting system. The samples were cultured for five days to allow cell adhesion and proliferation in 3D. At day 5, the samples were stained by DAPI/Phalloidin to examine the 3D cell network and morphology inside the 3D printed pattern. Figure 7E is a representative image that was obtained by stitching tiled images acquired with a fluorescence microscope with an automated stage. The images show that the cells proliferated well and filled most of the inside of the 3D mesh pattern. We further examined the details of the bioprinted EY-GelMA using a confocal microscope with 10X and 40X objectives (Figure 7F). The images revealed that the 3T3 cells reached high confluency inside the scaffolds after 5 days' culturing. Importantly, the cells formed 3D intercellular networks in the bioprinted EY GelMA pattern, which proved the high feasibility of using EY GelMA as a cell adhesive and visible light crosslinkable hydrogel for stereolithography bioprinting.

4. Conclusion

In this paper, we presented visible light crosslinkable and cell-adhesive gelatin methacryloyl hydrogels based on EY photoinitiation. Quantitative studies were conducted

to determine the critical concentration of EY required to crosslink different macromer concentrations of GelMA hydrogels, and the effect of EY concentration on the physical properties and biocompatibility of EY-GelMA hydrogels. It was found that the concentration EY positively affects the compressive Young's modulus of the EY-GelMA hydrogels, while it negatively affects the pore size of the microstructure, the mass swelling ratio, and cells' viability and proliferation. We printed EY-GelMA hydrogel patterns using the visible light-based SLA bioprinting system. Cells inside the bioprinted samples proliferated well to form 3D intercellular networks. Through a series of experiments, we demonstrated the great feasibility of the developed visible light crosslinkable and cell adhesive EY-GelMA hydrogels for biofabrication and tissue engineering applications.

Acknowledgement

This work was supported by a Natural Sciences and Engineering Research Council of Canada (NSERC) Discovery Grant (RGPIN-2014-04010) and Canada Foundation for Innovation John R. Evans Leaders Opportunity Fund.

References

[1] K.T. Nguyen, J.L. West, Photopolymerizable hydrogels for tissue engineering applications, Biomaterials. 23 (2002) 4307–4314. doi:10.1016/S0142-9612(02)00175-8.

[2] Z. Wang, S. Lee, K. Koo, K. Kim, Nanowire-Based Sensors for Biological and Medical Applications, IEEE Trans. Nanobioscience. 15 (2016) 186–199. doi:10.1109/TNB.2016.2528258.

[3] R. Dai, Z. Wang, R. Samanipour, K. Koo, K. Kim, Adipose-derived stem cells for tissue engineering and regenerative medicine applications, (n.d.).

[4] Z. Wang, R. Samanipour, K. Kim, Organ-on-a-Chip Platforms for Drug Screening and Tissue Engineering, in: Biomed. Eng. Front. Res. Converging Technol., Springer International Publishing, 2015: pp. 209–233.

[5] F.R. De Gruijl, H.J. Van Kranen, L.H.F. Mullenders, UV-induced DNA damage, repair, mutations and oncogenic pathways in skin cancer, J. Photochem. Photobiol. B Biol. 63 (2001) 19–27. doi:10.1016/S1011-1344(01)00199-3.

[6] R.P. Sinha, D.P. Häder, UV-induced DNA damage and repair: a review., Photochem. Photobiol. Sci. 1 (2002) 225–236. doi:10.1039/b201230h.

[7] B.K. Armstrong, A. Kricker, The epidemiology of UV induced skin cancer, J. Photochem. Photobiol. B Biol. 63 (2001) 8–18. doi:10.1016/S1011-1344(01)00198-1.

[8] B.D. Fairbanks, M.P. Schwartz, C.N. Bowman, K.S. Anseth, Photoinitiated polymerization of PEG-diacrylate with lithium phenyl-2,4,6-trimethylbenzoylphosphinate: polymerization rate and cytocompatibility, Biomaterials. 30 (2009) 6702–6707. doi:10.1016/j.biomaterials.2009.08.055.

[9] Z. Wang, X. Jin, R. Dai, J.F. Holzman, K. Kim, An ultrafast hydrogel photocrosslinking method for direct laser bioprinting, RSC Adv. 6 (2016) 21099–21104. doi:10.1039/C5RA24910D.

[10] S. Smith, M. Maclean, S.J. MacGregor, J.G. Anderson, M.H. Grant, Exposure of 3T3 mouse Fibroblasts and Collagen to High Intensity Blue Light, IFMBE Proc. 23 (2009) 1352–1355. doi:10.1007/978-3-540-92841-6_333.

[11] C.S. Bahney, T.J. Lujan, C.W. Hsu, M. Bottlang, J.L. West, B. Johnstone, Visible light photoinitiation of mesenchymal stem cell-laden bioresponsive hydrogels, Eur. Cells Mater. 22 (2011) 43–55.

[12] Z. Wang, R. Abdulla, B. Parker, R. Samanipour, S. Ghosh, K. Kim, A simple and high-resolution stereolithography-based 3D bioprinting system using visible light crosslinkable bioinks, Biofabrication. 7 (2015) 45009.

[13] B.M. Gumbiner, Cell adhesion: The molecular basis of tissue architecture and morphogenesis, Cell. 84 (1996) 345–357. doi:10.1016/S0092-8674(00)81279-9.

[14] R.O. Hynes, Integrins: versatility, modulation, and signaling in cell adhesion., Cell. 69 (1992) 11–25. doi:10.1016/0092-8674(92)90115-S.

[15] R. McBeath, D.M. Pirone, C.M. Nelson, K. Bhadriraju, C.S. Chen, Cell shape, cytoskeletal tension, and RhoA regulate stem cell lineage commitment, Dev. Cell. 6 (2004) 483–495. doi:10.1016/S1534-5807(04)00075-9.

[16] S. V Murphy, A. Atala, 3D bioprinting of tissues and organs., Nat. Biotechnol. 32 (2014) 773–785. doi:10.1038/nbt.2958.

[17] C. Mandrycky, Z. Wang, K. Kim, D.H. Kim, 3D bioprinting for engineering complex tissues, Biotechnol. Adv. 34 (2016) 422–434. doi:10.1016/j.biotechadv.2015.12.011.

[18] X. Cui, K. Breitenkamp, M.G. Finn, M. Lotz, D.D. D'Lima, Direct human cartilage repair using three-dimensional bioprinting technology., Tissue Eng. Part A. 18 (2012) 1304–12. doi:10.1089/ten.TEA.2011.0543.

[19] L.E. Bertassoni, M. Cecconi, V. Manoharan, M. Nikkhah, J. Hjortnaes, A.L. Cristino, G. Barabaschi, D. Demarchi, M.R. Dokmeci, Y. Yang, A. Khademhosseini, Hydrogel bioprinted microchannel networks for vascularization of tissue engineering constructs., Lab Chip. 14 (2014) 2202–11. doi:10.1039/c4lc00030g.

[20] M.J. Sawkins, P. Mistry, B.N. Brown, K.M. Shakesheff, L.J. Bonassar, J. Yang, Cell and protein compatible 3D bioprinting of mechanically strong constructs for bone repair., Biofabrication. 7 (2015) 35004. doi:10.1088/1758-5090/7/3/035004.

[21] D.B. Kolesky, R.L. Truby, A.S. Gladman, T.A. Busbee, K.A. Homan, J.A. Lewis, 3D bioprinting of vascularized, heterogeneous cell-laden tissue constructs., Adv.

Mater. 26 (2014) 3124–30. doi:10.1002/adma.201305506.

[22] D.B. Kolesky, K.A. Homan, M.A. Skylar-Scott, J.A. Lewis, Three-dimensional bioprinting of thick vascularized tissues, Proc. Natl. Acad. Sci. (2016) 201521342. doi:10.1073/pnas.1521342113.

[23] P. Zorlutuna, J.H. Jeong, H. Kong, R. Bashir, Stereolithography-based hydrogel microenvironments to examine cellular interactions, Adv. Funct. Mater. 21 (2011) 3642–3651. doi:10.1002/adfm.201101023.

[24] R. Gauvin, Y.-C. Chen, J.W. Lee, P. Soman, P. Zorlutuna, J.W. Nichol, H. Bae, S. Chen, A. Khademhosseini, Microfabrication of complex porous tissue engineering scaffolds using 3D projection stereolithography., Biomaterials. 33 (2012) 3824–34. http://www.sciencedirect.com/science/article/pii/S0142961212000944 (accessed December 26, 2015).

[25] T.Q. Huang, X. Qu, J. Liu, S. Chen, 3D printing of biomimetic microstructures for cancer cell migration., Biomed. Microdevices. 16 (2014) 127–32. doi:10.1007/s10544-013-9812-6.

[26] X. Ma, X. Qu, W. Zhu, Y.-S. Li, S. Yuan, H. Zhang, J. Liu, P. Wang, C.S.E. Lai, F. Zanella, G.-S. Feng, F. Sheikh, S. Chien, S. Chen, Deterministically patterned biomimetic human iPSC-derived hepatic model via rapid 3D bioprinting, Proc. Natl. Acad. Sci. 113 (2016) 201524510. doi:10.1073/pnas.1524510113.

[27] H. Lin, D. Zhang, P.G. Alexander, G. Yang, J. Tan, A.W.M. Cheng, R.S. Tuan,

Application of visible light-based projection stereolithography for live cell-scaffold fabrication with designed architecture, Biomaterials. 34 (2013) 331–339. doi:10.1016/j.biomaterials.2012.09.048.

[28] J.W. Nichol, S.T. Koshy, H. Bae, C.M. Hwang, S. Yamanlar, A. Khademhosseini, Cell-laden microengineered gelatin methacrylate hydrogels., Biomaterials. 31 (2010) 5536–44. doi:10.1016/j.biomaterials.2010.03.064.

[29] X.-H. Qin, A. Ovsianikov, J. Stampfl, R. Liska, Additive manufacturing of photosensitive hydrogels for tissue engineering applications, BioNanoMaterials. 15 (2014) 49–70. doi:10.1515/bnm-2014-0008.

[30] G. Ullrich, P. Burtscher, U. Salz, N. Moszner, R. Liska, Phenylglycine derivatives as coinitiators for the radical photopolymerization of acidic aqueous formulations, J. Polym. Sci. Part A Polym. Chem. 44 (2006) 115–125. doi:10.1002/pola.21139.

[31] C.B. Hutson, J.W. Nichol, H. Aubin, H. Bae, S. Yamanlar, S. Al-Haque, S.T. Koshy, A. Khademhosseini, Synthesis and characterization of tunable poly(ethylene glycol): gelatin methacrylate composite hydrogels., Tissue Eng. Part A. 17 (2011) 1713–23. doi:10.1089/ten.TEA.2010.0666.

[32] P. Kim, A. Yuan, K.-H. Nam, A. Jiao, D.-H. Kim, Fabrication of poly(ethylene glycol): gelatin methacrylate composite nanostructures with tunable stiffness and degradation for vascular tissue engineering., Biofabrication. 6 (2014) 24112. doi:10.1088/1758-5082/6/2/024112.

[33] P. Occhetta, R. Visone, L. Russo, L. Cipolla, M. Moretti, M. Rasponi, VA-086 methacrylate gelatine photopolymerizable hydrogels: A parametric study for highly biocompatible 3D cell embedding, J. Biomed. Mater. Res. - Part A. 103 (2015) 2109–2117. doi:10.1002/jbm.a.35346.

[34] H.A. Awad, M.Q. Wickham, H.A. Leddy, J.M. Gimble, F. Guilak, Chondrogenic differentiation of adipose-derived adult stem cells in agarose, alginate, and gelatin scaffolds, Biomaterials. 25 (2004) 3211–3222. doi:10.1016/j.biomaterials.2003.10.045.

[35] N.A. Peppas, J.Z. Hilt, A. Khademhosseini, R. Langer, Hydrogels in biology and medicine: From molecular principles to bionanotechnology, Adv. Mater. 18 (2006) 1345–1360. doi:10.1002/adma.200501612.

[36] F.J. O'Brien, B. a Harley, M. a Waller, I. V Yannas, L.J. Gibson, P.J. Prendergast, The effect of pore size on permeability and cell attachment in collagen scaffolds for tissue engineering., Technol. Health Care. 15 (2007) 3–17.

[37] K. Yue, G. Trujillo-De Santiago, M. Mois Es Alvarez, A. Tamayol, N. Annabi, A. Khademhosseini, Synthesis, properties, and biomedical applications of gelatin methacryloyl (GelMA) hydrogels, Biomaterials. 73 (2015) 254–271. doi:10.1016/j.biomaterials.2015.08.045.

[38] Z. Wang, Z. Tian, F. Menard, K. Kim, Comparative study of gelatin methacrylate hydrogels from different sources for biofabrication applications, Biofabrication.

(2017). doi:10.1088/1758-5090/aa83cf.

[39] C.M. Murphy, M.G. Haugh, F.J. O'Brien, The effect of mean pore size on cell attachment, proliferation and migration in collagen-glycosaminoglycan scaffolds for bone tissue engineering, Biomaterials. 31 (2010) 461–466. doi:10.1016/j.biomaterials.2009.09.063.

[40] H.J. Yoon, S.R. Shin, J.M. Cha, S.-H. Lee, J.-H. Kim, J.T. Do, H. Song, H. Bae, Cold Water Fish Gelatin Methacryloyl Hydrogel for Tissue Engineering Application, PLoS One. 11 (2016) e0163902. doi:10.1371/journal.pone.0163902.

[41] H. Qi, Y. Du, L. Wang, H. Kaji, H. Bae, A. Khademhosseini, Patterned differentiation of individual embryoid bodies in spatially organized 3D hybrid microgels, Adv. Mater. 22 (2010) 5276–5281. doi:10.1002/adma.201002873.

[42] G. Gao, A.F. Schilling, K. Hubbell, T. Yonezawa, D. Truong, Y. Hong, G. Dai, X. Cui, Improved properties of bone and cartilage tissue from 3D inkjet-bioprinted human mesenchymal stem cells by simultaneous deposition and photocrosslinking in PEG-GelMA, Biotechnol. Lett. 37 (2015) 2349–2355. doi:10.1007/s10529-015-1921-2.

[43] E. Cukierman, Taking Cell-Matrix Adhesions to the Third Dimension, Science (80-.). 294 (2001) 1708–1712. doi:10.1126/science.1064829.

[44] M.W. Tibbitt, K.S. Anseth, Hydrogels as extracellular matrix mimics for 3D cell culture, Biotechnol. Bioeng. 103 (2009) 655–663. doi:10.1002/bit.22361.

[45] F. Masson, C. Decker, S. Andre, X. Andrieu, UV-curable formulations for UV-transparent optical fiber coatings: I. Acrylic resins, Prog. Org. Coatings. 49 (2004) 1–12. doi:10.1016/S0300-9440(03)00122-X.

Tables

Table 1. Comparison of widely used photoinitiators in tissue engineering

Chemical name	Abbreviation	Absorbing peak	Sources
1-[4-(2-hydroxyethoxy)-phenyl]-2-hydroxy-2-methyl-1-propanone	Irgacure 2959	257 nm	[29,45]
Lithium phenyl-2,4,6-trimethylbenzoylphosphinate	LAP	375 nm	[27,29]
2,2'-azobis[2-methyl-n-(2-hydroxyethyl)propionamide]	VA-086	385 nm	[33]
2′,4′,5′,7′-tetrabromofluorescein disodium salt	Eosin Y	514 nm	[11,29]

Table 2. Five different EY based GelMA prepolymer solutions

Name	GelMA	Eosin Y	TEA	NVP	Abbreviation
10% w/v GelMA with 4X concentrated EY initiator	10% w/v	0.04 mM	0.4% w/v	148 nM	4X 10% GelMA
15% w/v GelMA with 2X concentrated EY initiator	15% w/v	0.02 mM	0.2% w/v	74 nM	2X 15% GelMA
15% w/v GelMA with 3X concentrated EY initiator	15% w/v	0.03 mM	0.3% w/v	111 nM	3X 15% GelMA
15% w/v GelMA with 4X concentrated EY initiator	15% w/v	0.04 mM	0.4% w/v	148 nM	4X 15% GelMA
20% w/v GelMA with 1X concentrated EY initiator	20% w/v	0.01 mM	0.1% w/v	37 nM	1X 20% GelMA

Table 3. Crosslinkability of GelMA hydrogel using EY photoinitiation

	1X EY	2X EY	4X EY
10% w/v GelMA	N	N	Y
15% w/v GelMA	N	Y	Y
20% w/v GelMA	Y	Y	Y

Note: “Y” means that GelMA is crosslinked within 20 minutes and “N” means that GelMA cannot be crosslinked within 20 minutes.

Figures

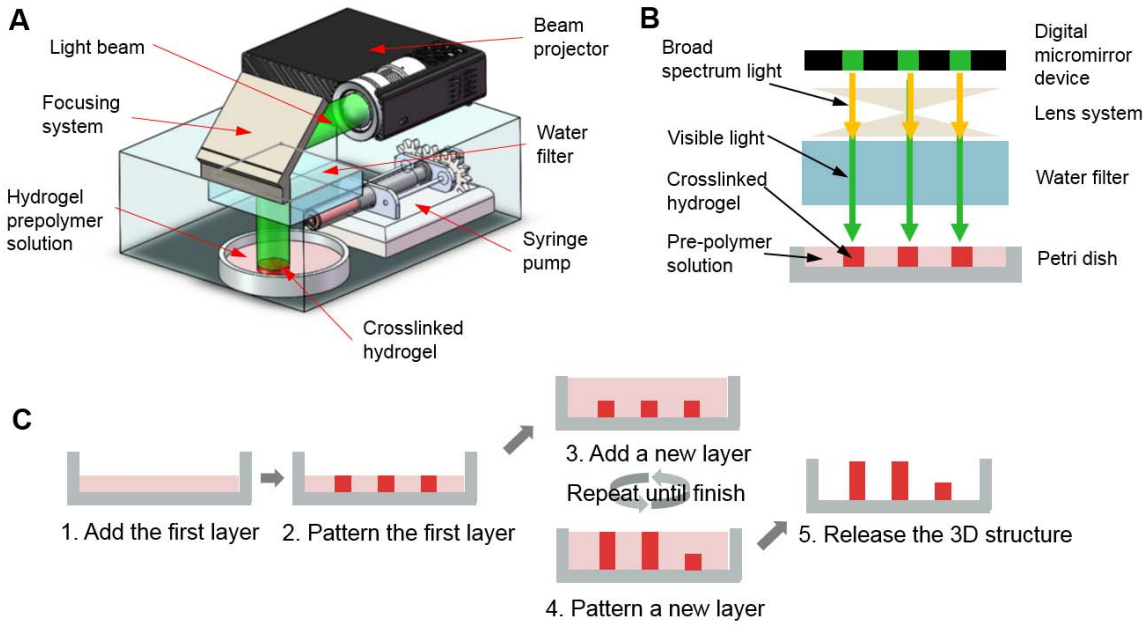

Figure 1. Visible light-based stereolithography 3D bioprinting system. (A) Scheme of the SLA bioprinting system with various components. (B) Working principles of single-layer printing. (C) Multiple layers printing process.

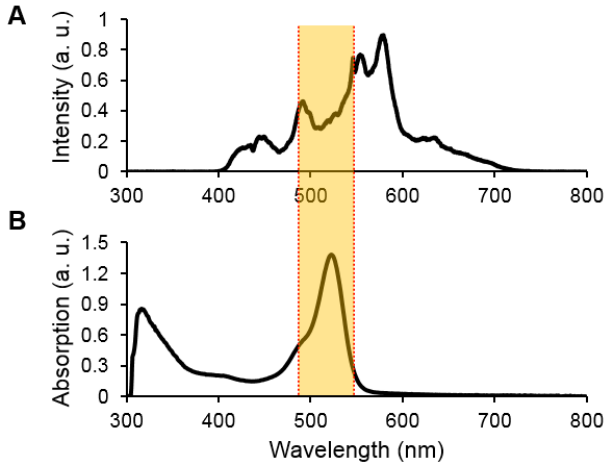

Figure 2. Spectral analysis of the beam projector and EY photoinitiator. (A) The spectrum of visible light emitted by the beam projector. (B) The UV-visible absorption spectrum of the EY-based photoinitiator.

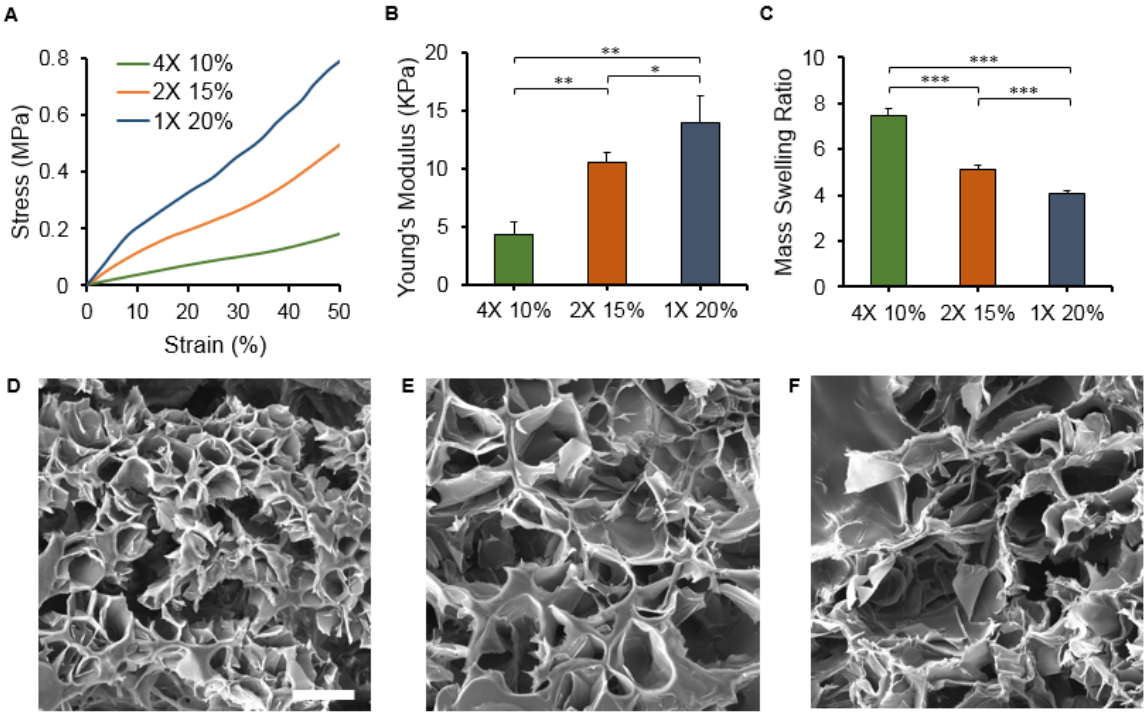

Figure 3. Characterization of EY-GelMA's physical properties: Effect of varying GelMA concentrations with the minimal amounts of EY. (A) Strain-stress curves for three different combinations of EY-GelMAs. (B) Compressive Young's Modulus; $n = 5$. (C) Equilibrium mass swelling ratio. (D-E) Scanning electron microscope images of (D) 4X EY 10% GelMA, (E) 2X EY 15% and (F) 1X EY 20% GelMA. Scale bar = 100 μm; *p < 0.05, **p < 0.01, and ***p < 0.001.

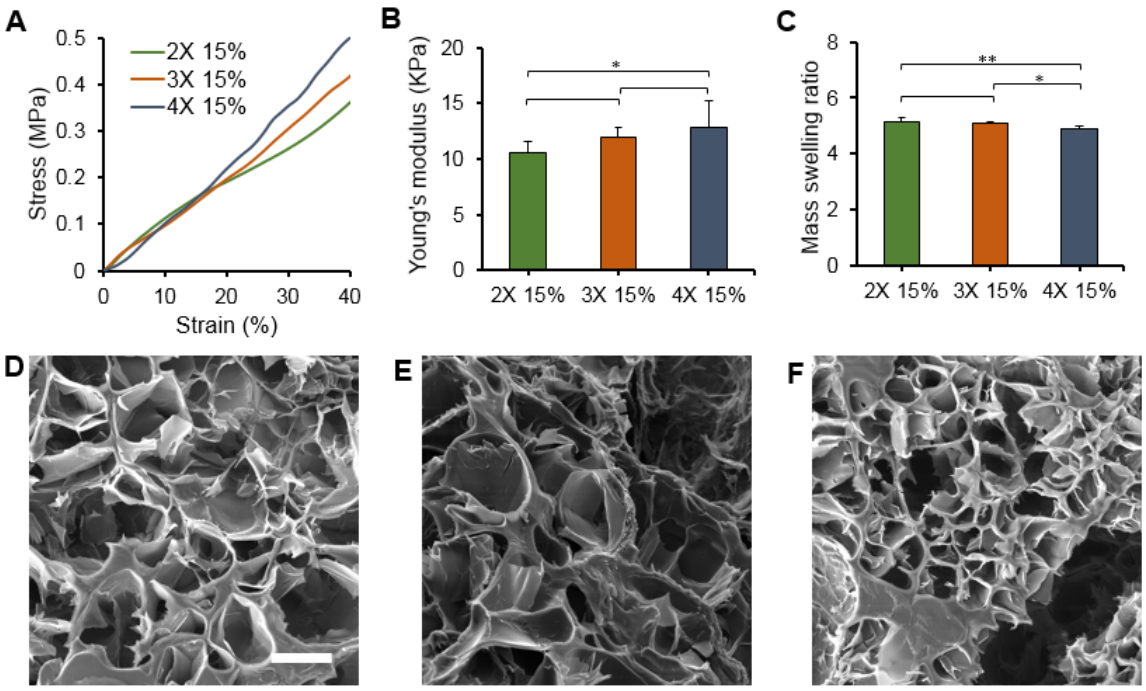

Figure 4. Characterization of EY-GelMA's physical properties: Effect of varying EY concentrations. (A) Strain-stress curves for three different combinations of EY-GelMAs. (B) Compressive Young's Modulus; n = 5. (C) Equilibrium mass swelling ratio. (D-E) Scanning electron microscope images of (D) 2X Eo Y 15% GelMA, (E) 3X EY 15% and (F) 4X EY 15% GelMA. Scale bar = 100 µm, *p < 0.05, **p < 0.01, and ***p < 0.001.

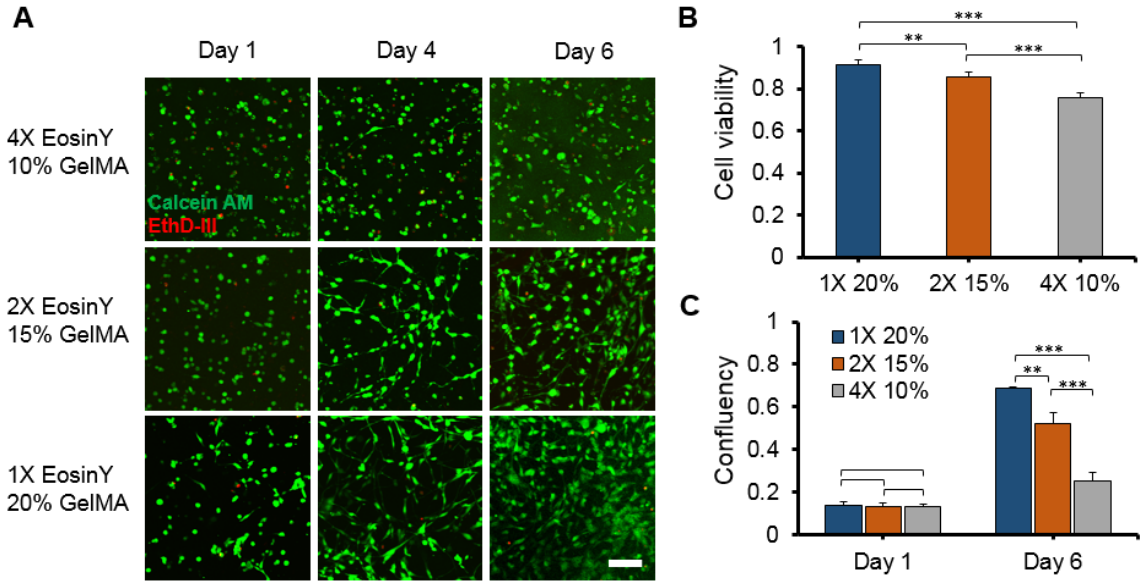

Figure 5. Evaluation of biocompatibility: Effect of varying GelMA concentrations with the minimal amounts of EY. (A) Representative images showing live cells (green: Calcein AM) and dead cells (red: EthD-II). Images were acquired at day 1, 4 and 6 with reagents combinations of 4X 10%, 2X 15% and 1X 20% EY-GelMAs. (B) Comparison of cell viability at day 1 with selected reagent combinations; n = 5. (C) Comparison of cell confluency at day 1 and 6 with selected reagent combinations; n = 5. Scale bar = 100 μm; *p < 0.05, **p < 0.01, and ***p < 0.001.

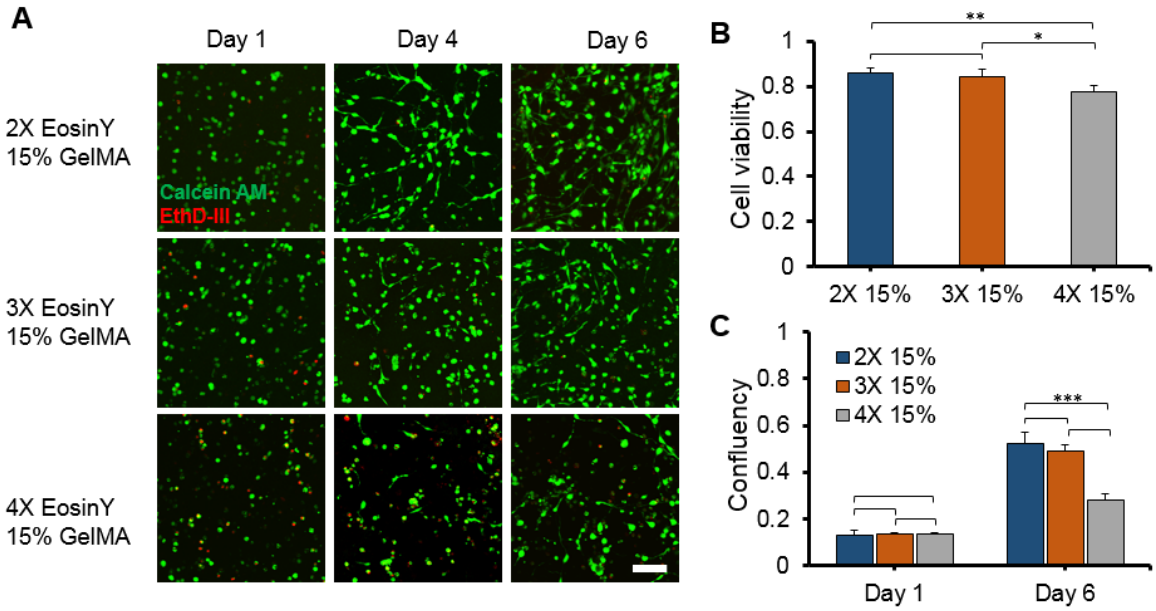

Figure 6. Effect EY concentration on cell viability and adhesion. (A) Representative images showing live cells (green: Calcein AM) and dead cells (red: EthD-II). Images were acquired at day 1, 4 and 6 with reagents combinations of 2X 15%, 3X 15% and 4X 15% EY-GelMAs. (B) Effect of EY concentration on cell viability at day 1; n = 5. (C) Comparison of cell confluency at day 1 and 6 with varying EY concentrations; n = 5. Scale bar = 100 μm; *p < 0.05, **p < 0.01, and ***p < 0.001.

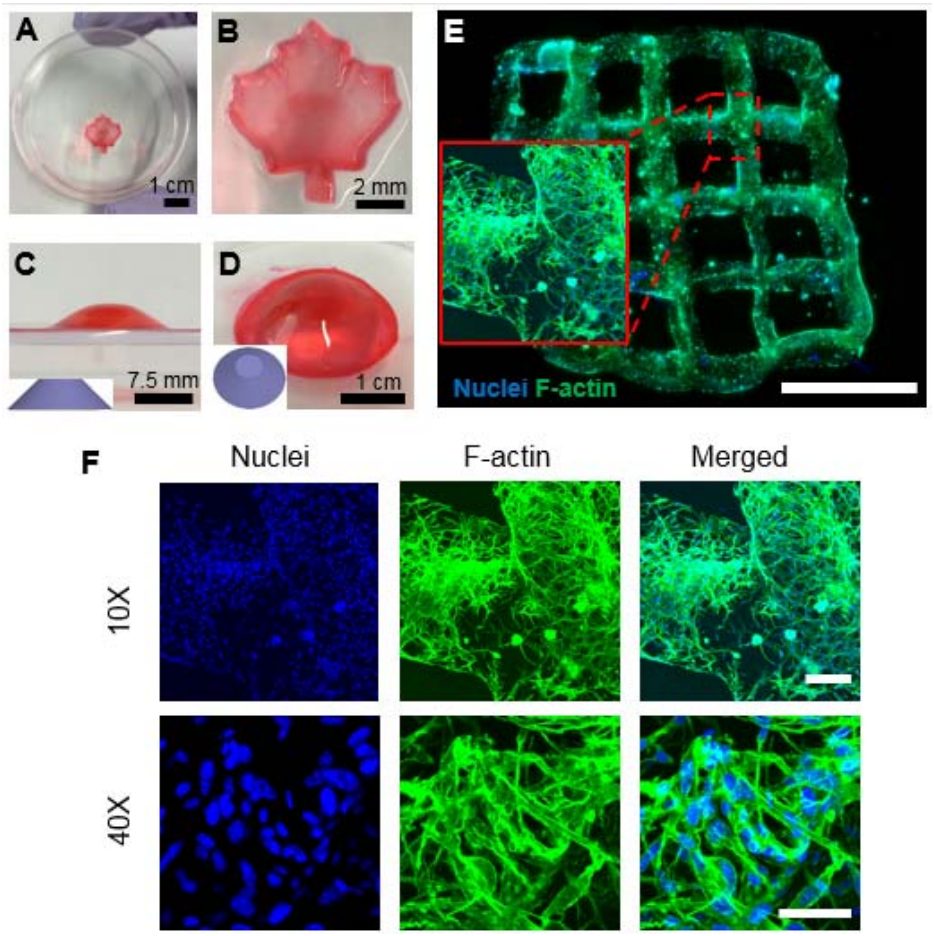

Figure 7. Examples of 3D bioprinted cellular networks. All experiments used a bioink with the optimized reagents ratio (2X EY 15% GelMA). (A, B) Maple leaf pattern. (C, D) Truncated cone structure photographed from the side (C) and from the top (D). Insets depict the programmed geometry with matching view angles. (E) NIH-3T3 cell-laden bioprinted sample at day 5 stained with DAPI for nuclei (blue) and Phalloidin 488 for F-actin (green). The image was constructed by stitching tiled fluorescence images of the mesh pattern. Scale bar = 2 mm. (F) Confocal fluorescence microscopy images of a junction in the mesh pattern at 10X and 40X magnification. Scale bars = 300 μm (10X) and 50 μm (40X).